Dual-Model Pharmacokinetic Simulation of Rapamycin (Sirolimus): Population PK and PBPK Side by Side

exp-012*
Edison Scientific

March 2026

Abstract

Sirolimus (rapamycin) has complex pharmacokinetics: low oral bioavailability (∼15%), extreme erythrocyte sequestration (blood-to-plasma ratio ∼35:1), extensive CYP3A4-mediated metabolism, and drug–drug interactions spanning 10-fold exposure ranges. We constructed two pharmacokinetic models from published clinical data — a two-compartment population PK (PopPK) model and a simplified whole-body PBPK model — implemented both in `mrgsolve`, and ran them against identical clinical inputs. Under standard conditions (2 mg QD, 70 kg, no DDI), both models converge on steady-state average exposure ($C_{avg} \approx 6.7$ ng/mL, $AUC_\tau \approx 160$ ng·h/mL) but diverge in peak-trough amplitude: the PopPK model predicts wider fluctuation (C_{max} 16.3 vs. 11.5 ng/mL; C_{trough} 2.5 vs. 5.9 ng/mL). DDI simulations show ketoconazole driving trough concentrations to 41 ng/mL (vs. 2.5 ng/mL baseline), while rifampin reduces them to 0.1 ng/mL. Population simulation (n=200) demonstrates 3-fold variability in trough levels, with only 20% of virtual patients within the transplant therapeutic window at 2 mg QD without dose adjustment. The interactive Shiny application is available for research use.

1 Introduction

Rapamycin (sirolimus) was approved as an immunosuppressant for renal transplant recipients in 1999. Its pharmacokinetics are difficult to model for several intersecting reasons. Oral bioavailability is approximately 14–17%, driven primarily by extensive gut wall first-pass extraction via CYP3A4 ($F_g \approx 0.16$), with relatively low hepatic extraction ($F_h \approx 0.96$–0.98) [Emoto et al., 2013, Zimmerman and Kahan, 1997]. Sirolimus concentrates heavily in erythrocytes via binding to the intracellular immunophilin FKBP12, yielding a blood-to-plasma ratio of approximately 35:1 at therapeutic concentrations [Mahalati and Kahan, 2001, ter Heine et al., 2018]. The terminal half-life is long (∼60 hours), and CYP3A4/3A5-mediated DDIs produce exposure changes spanning an order of magnitude [Zimmerman, 2004b].

These properties create an interesting dual-model test case: a drug where empirical (PopPK) and mechanistic (PBPK) approaches should agree on average exposure but may diverge on tissue distribution, peak-trough fluctuation, and DDI prediction. We built both and deployed them in an interactive application.

*Edison Scientific. Correspondence: exp-012@edison.science

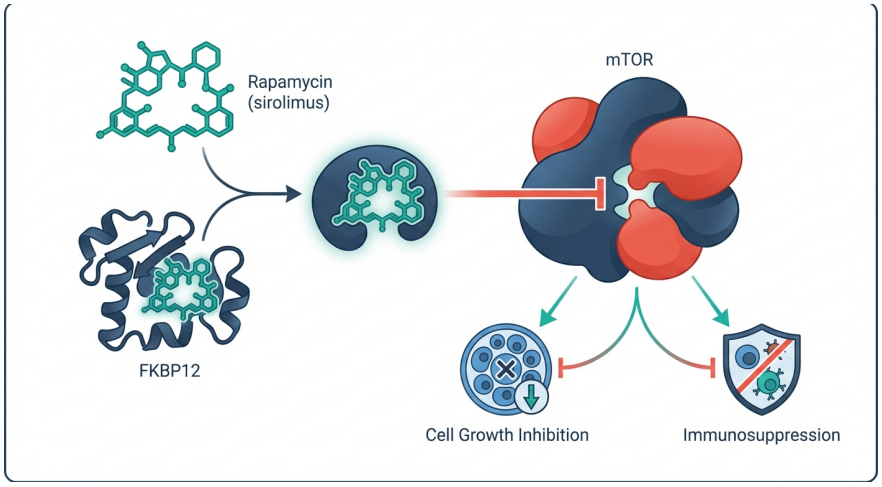

Figure 1: Rapamycin mechanism of action. The drug binds FKBP12 intracellularly; the rapamycin–FKBP12 complex inhibits mTORC1, suppressing cell growth and proliferation. The same FKBP12 binding drives ∼95% erythrocyte sequestration.

2 Methods

2.1 Literature Synthesis

Pharmacokinetic data were compiled from published PopPK analyses, PBPK models, clinical pharmacology reviews, and DDI studies using the Edison Scientific literature platform. Four systematic searches covered: (1) human and animal PK data, (2) existing PopPK and PBPK models, (3) modeling methodology for CYP3A substrates with erythrocyte binding, and (4) rapalog (everolimus, temsirolimus) PK for cross-compound validation. Over 40 primary sources were reviewed.

2.2 Model 1: Population PK (2-Compartment)

The PopPK model uses a two-compartment structure with first-order absorption, parameterized on whole-blood concentrations (Figure 2). Parameters from Golubović et al. (2019) [Golubović et al., 2019]: $CL/F = 12.2$ L/h, $V_c/F = 118$ L, $V_p/F = 609$ L, $Q/F = 5.07$ L/h, $k_a = 2.19$ h^{-1}.

Covariate effects:

- **Body weight:** Allometric scaling (exponent 0.75 on clearances, 1.0 on volumes) [Ferron et al., 1997].
- **Hematocrit:** Inverse power on CL/F (exponent 0.67), reflecting RBC-mass dependence [Wu et al., 2012, Mao et al., 2024].
- **CYP3A5 genotype:** $CL/F = CL_{TV} \times (1 + 0.97 \times \text{CYP3A5})$, approximately doubling clearance in expressers [Lukas et al., 2010].
- **DDI:** Fold-change on CL/F from clinical DDI studies [Zimmerman, 2004b].
- **Hepatic impairment:** Scalar reduction on CL/F from Child-Pugh studies [Zimmerman et al., 2005, 2008].
- **Blood-to-plasma:** Fixed $B{:}P = 35$ [Emoto et al., 2013, Mahalati and Kahan, 2001].

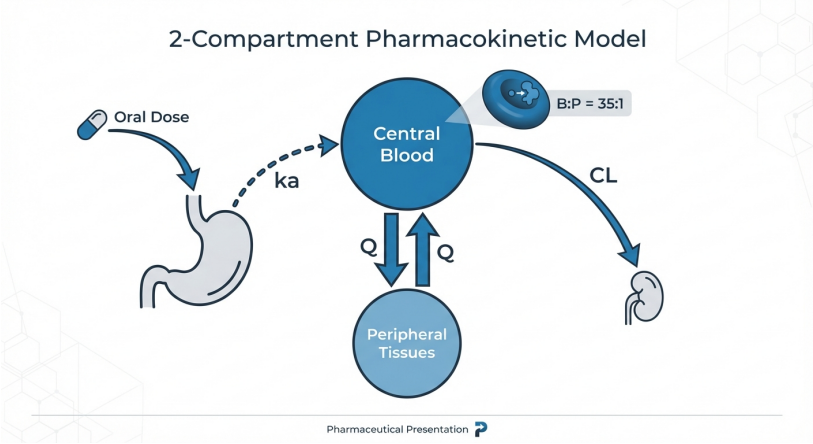

Figure 2: Two-compartment PopPK model. Oral dose absorbed (k_a) into central blood compartment, bidirectional exchange (Q) with peripheral, elimination (CL) from central. B:P $\approx$ 35:1 from FKBP12-mediated erythrocyte binding.

2.3 Model 2: Simplified PBPK

The PBPK model uses a perfusion-limited, whole-body structure (Figure 3) parameterized from the Simcyp model of Emoto et al. (2013) [Emoto et al., 2013]:

- **Absorption:** $k_a = 2.77$ h^{-1} [Ferron et al., 1997], $F_a = 0.95$, pre-systemic $F_g = 0.16$.
- **Hepatic clearance:** Well-stirred model, $CL_{int} = 1.78$ L/h, yielding $F_h \approx 0.98$.
- **Tissue distribution:** Liver $K_p = 3$, adipose $K_p = 28$ ($\log P = 4.3$), muscle $K_p = 0.5$, kidney $K_p = 2$, rest $K_p = 1$.
- **Physiology:** Cardiac output 390 L/h (70 kg), organ blood flows and volumes scaled allometrically.
- **DDI mechanism:** Fold-changes on CL_{int} and gut wall extraction.
- **CYP3A5:** 24% increase in CL_{int} for expressers [Emoto et al., 2015].

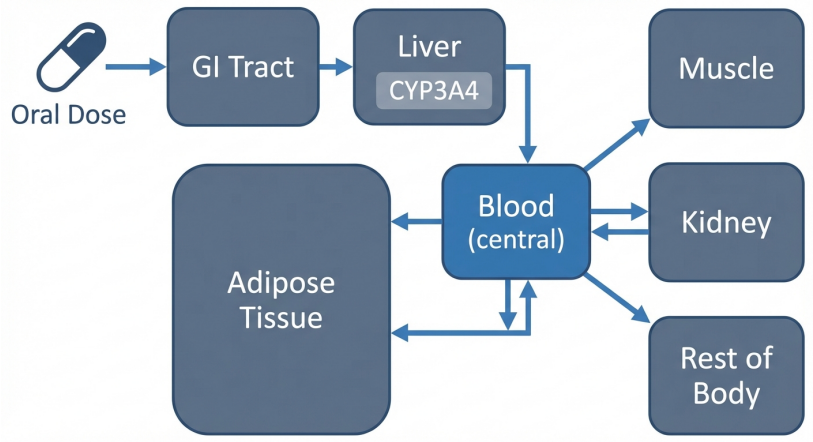

Figure 3: Simplified whole-body PBPK model. Gut wall first-pass (CYP3A4, $F_g \approx 0.16$), hepatic clearance (well-stirred), perfusion-limited tissue distribution to adipose ($K_p = 28$), muscle, kidney, and rest of body.

2.4 Implementation

Both models were coded as C++ ODE systems in `mrgsolve` and deployed in R/Shiny (`bslib` framework). Time step: 0.5 h. Population simulations: 200 virtual patients with log-normal IIV on CL/F (CV 38%), V_c/F (32%), V_p/F (26%).

3 Results

3.1 Model Comparison Under Standard Conditions

Figure 4 shows overlaid concentration–time profiles for both models under standard conditions (2 mg QD, 70 kg, HCT 0.40, CYP3A5 non-expresser, no DDI, 30 days). Table 1 reports steady-state metrics from the final dosing interval.

Both models predict nearly identical average exposure ($C_{avg} \approx 6.7$ ng/mL, $AUC_\tau \approx 160$ ng·h/mL). This convergence is expected: both are calibrated against the same observed clearance (∼12 L/h) and bioavailability (∼15%).

The key difference is peak-trough amplitude. The PopPK model, with its two-compartment empirical structure, predicts sharper peaks ($C_{max} = 16.3$ ng/mL) and deeper troughs ($C_{trough} = 2.5$ ng/mL). The PBPK model's multi-organ tissue distribution buffers the central compartment, producing flatter profiles ($C_{max} = 11.5$ ng/mL, $C_{trough} = 5.9$ ng/mL). This structural difference has clinical implications: the PopPK model suggests more patients will dip below the 5 ng/mL transplant target at trough, while the PBPK model predicts more sustained exposure.

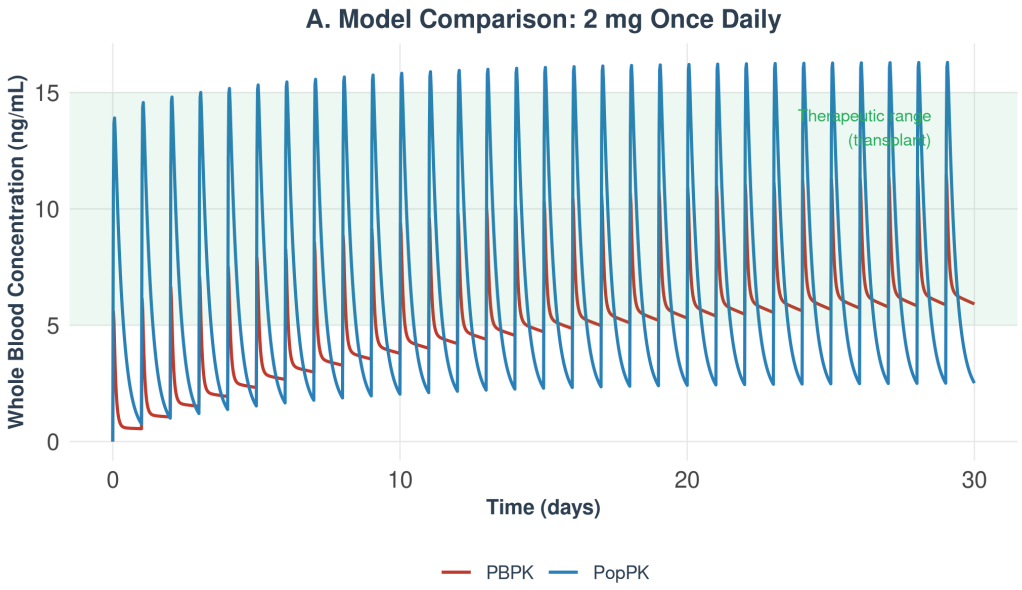

Figure 4: PopPK vs. PBPK concentration–time profiles over 30 days of 2 mg QD dosing. Green band: transplant therapeutic range (5–15 ng/mL). Both models converge on average exposure but differ in peak-trough amplitude.

Table 1: Steady-state pharmacokinetic metrics from the final dosing interval (2 mg QD, day 29–30). Both models agree on average exposure; the PopPK model shows wider peak-trough fluctuation.

Model	C_{max} **(ng/mL)**	C_{trough} **(ng/mL)**	C_{avg} **(ng/mL)**	AUC_{τ} **(ng·h/mL)**
PopPK (2-Compartment)	16.30	2.51	6.68	160
PBPK (Mechanistic)	11.45	5.88	6.65	160
Ratio (PopPK/PBPK)	**1.42**	**0.43**	**1.00**	**1.00**

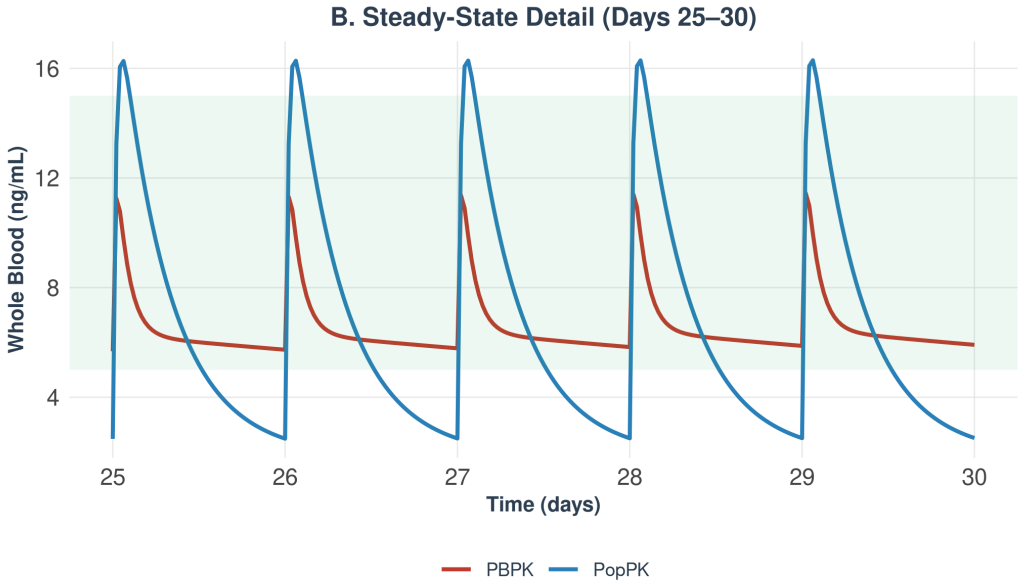

Figure 5: Steady-state detail (days 25–30). The PopPK model shows pronounced peak-trough cycling while the PBPK model predicts a more damped profile due to tissue buffering.

3.2 Bioavailability Cascade

The PBPK model decomposes oral bioavailability into its physiological components (Table 2). The dominant bottleneck is gut wall CYP3A4 metabolism, which eliminates 84% of absorbed drug. Hepatic extraction is minimal (∼2%). This decomposition explains why CYP3A4 inhibitors produce such large exposure increases: they relieve the gut wall bottleneck, not hepatic clearance.

Table 2: PBPK bioavailability cascade. Gut wall CYP3A4 metabolism is the dominant source of low oral bioavailability.

Step	**Availability**	**% Drug Lost**	**Mechanism**
Absorption (F_a)	0.950	5%	High intestinal permeability
Gut wall (F_g)	0.160	84%	CYP3A4 first-pass metabolism
Hepatic (F_h)	0.980	2%	Low hepatic extraction ratio
Overall (F)	**0.149**	**85%**	$F = F_a \times F_g \times F_h$

3.3 Drug–Drug Interactions

Figure 6 overlays all DDI scenarios on a log-scale plot. Table 3 reports the simulated steady-state metrics alongside clinically observed AUC fold-changes.

The strongest interactions are with ketoconazole and voriconazole, which drive steady-state trough concentrations from 2.5 ng/mL (baseline) to 41–43 ng/mL — well above the therapeutic ceiling and consistent with the clinical contraindication. Erythromycin produces an intermediate effect (C_{trough} 20.5 ng/mL), while diltiazem shows a modest interaction (C_{trough} 5.7 ng/mL). Rifampin induction reduces trough to 0.1 ng/mL, effectively eliminating therapeutic exposure.

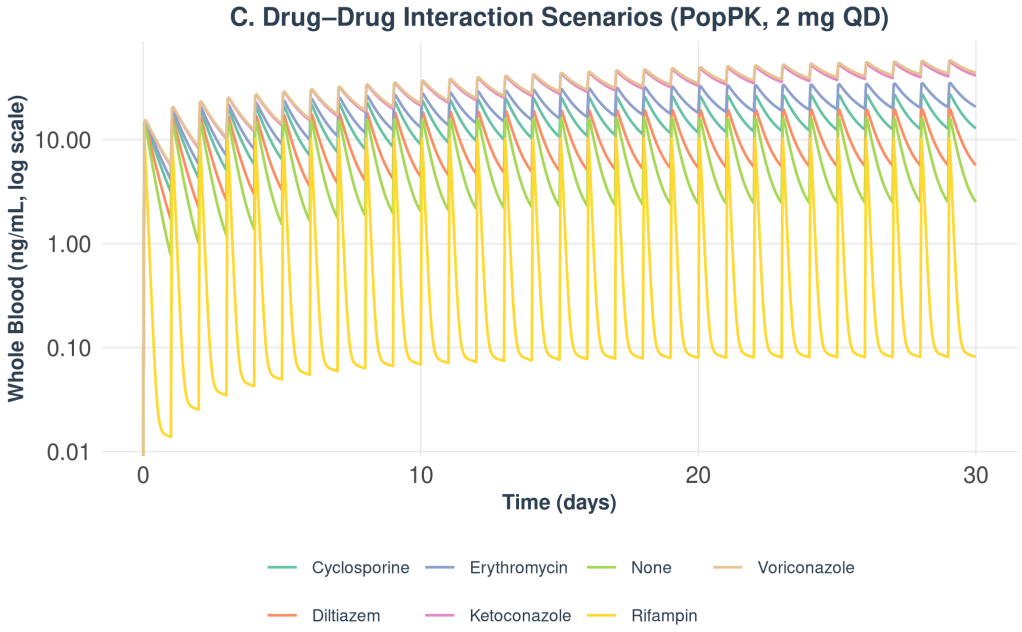

Figure 6: DDI scenario overlay (PopPK model, 2 mg QD, log scale). Strong CYP3A4 inhibitors increase steady-state concentrations by an order of magnitude; rifampin induction nearly abolishes exposure.

Table 3: Simulated steady-state metrics under DDI scenarios (PopPK, 2 mg QD, last dosing interval). Observed AUC fold-changes from Zimmerman 2004 [Zimmerman, 2004b].

Co-medication	C_{max} **(ng/mL)**	C_{trough} **(ng/mL)**	C_{avg} **(ng/mL)**	**Obs. AUC fold-Δ**	**Clinical significance**
None (baseline)	16.1	2.5	6.5	—	—
Ketoconazole	55.4	40.7	47.2	×10.9 ↑	Contraindicated
Voriconazole	58.1	43.3	50.0	×11.1 ↑	Contraindicated
Erythromycin	35.1	20.5	26.4	×4.4 ↑	Dose reduction
Diltiazem	19.5	5.7	10.5	×1.6 ↑	Monitor levels
Cyclosporine	27.1	12.8	18.3	×2–3 ↑	Per protocol
Rifampin	10.2	0.1	1.1	×0.18 ↓	Dose increase

3.4 Tissue Distribution

Figure 7 shows PBPK-predicted tissue concentrations. At steady state (day 30), adipose tissue reaches 183.5 ng/g — approximately 30-fold higher than blood (6.1 ng/mL). Liver concentrations are 17.8 ng/g (∼3× blood). This extensive adipose accumulation acts as a deep reservoir: during washout, adipose slowly releases drug back into the circulation, contributing to the long terminal half-life.

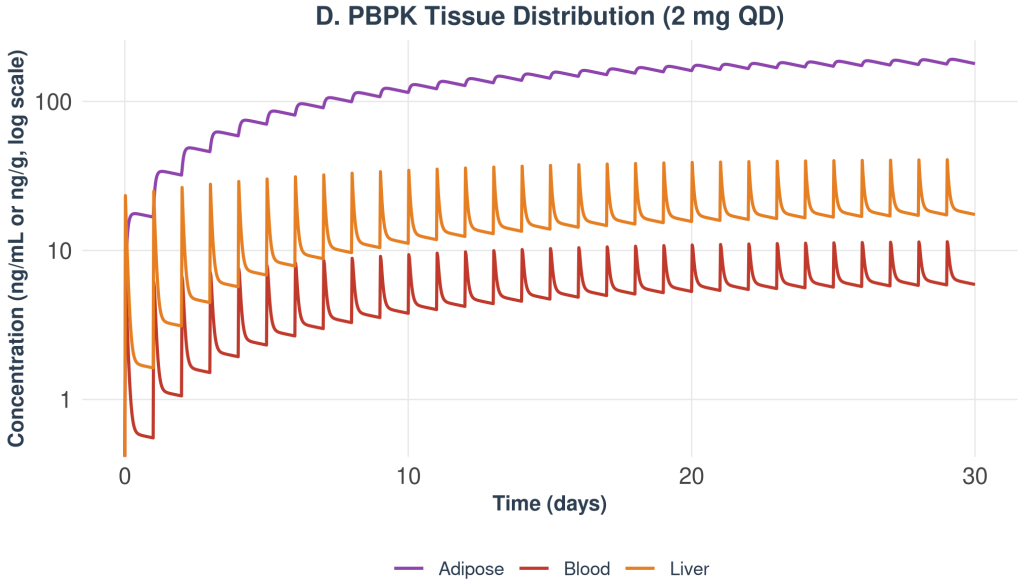

Figure 7: PBPK tissue concentrations over 30 days (log scale). Adipose tissue accumulates to ∼30-fold blood concentrations at steady state, consistent with sirolimus's high lipophilicity ($\log P = 4.3$) and published K_p values [Emoto et al., 2013].

3.5 Population Variability

Figure 8 shows the virtual population simulation (n=200, PopPK model). The 5th–95th percentile envelope spans approximately 3-fold around the median at steady state. Figure 9 shows the trough concentration distribution at day 30.

At 2 mg QD without dose individualization, only 20% of virtual patients achieve troughs within the transplant therapeutic window (5–15 ng/mL). The majority (80%) fall below 5 ng/mL. No patients exceed 15 ng/mL. This is consistent with clinical practice, where loading doses and TDM-guided adjustments are standard.

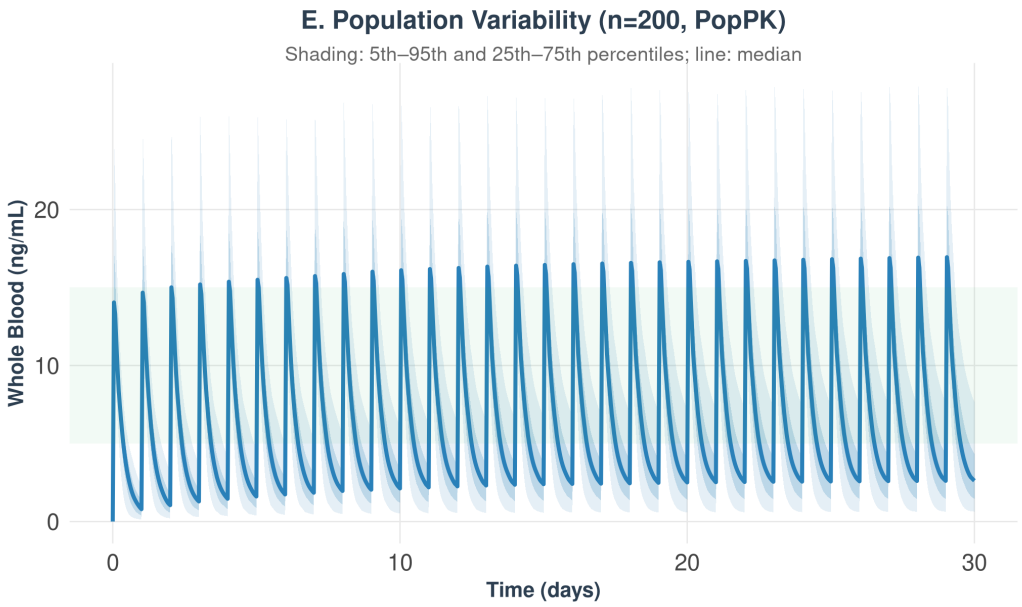

Figure 8: Population simulation (n=200, PopPK). Dark shading: 25th–75th percentiles; light shading: 5th–95th; line: median. Green band: therapeutic range.

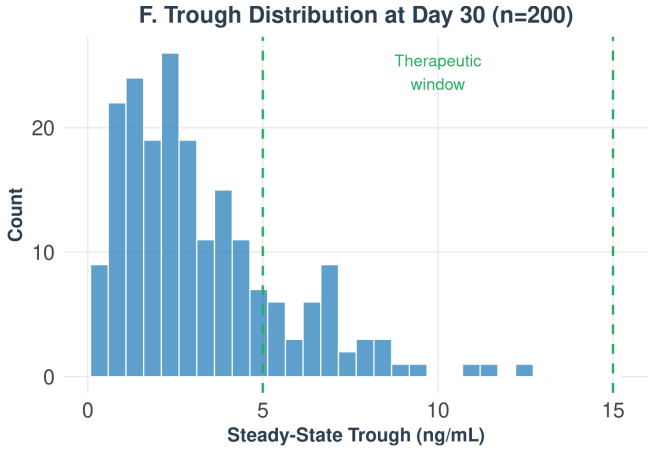

Figure 9: Distribution of steady-state trough concentrations at day 30 (n=200). Dashed green lines: transplant therapeutic window (5–15 ng/mL). At 2 mg QD, 80% of patients are sub-therapeutic without dose adjustment.

3.6 Covariate Sensitivity

Figure 10 and Table 4 show how CYP3A5 genotype and hepatic impairment alter steady-state PK. CYP3A5 expressers have approximately halved exposure (C_{avg} 3.2 vs. 6.5 ng/mL), reflecting their higher metabolic clearance. Child-Pugh B hepatic impairment increases C_{avg} by 57% (to 10.2 ng/mL), while Child-Pugh C nearly doubles it (to 14.1 ng/mL). These covariate effects are large enough to require dose adjustment in clinical practice.

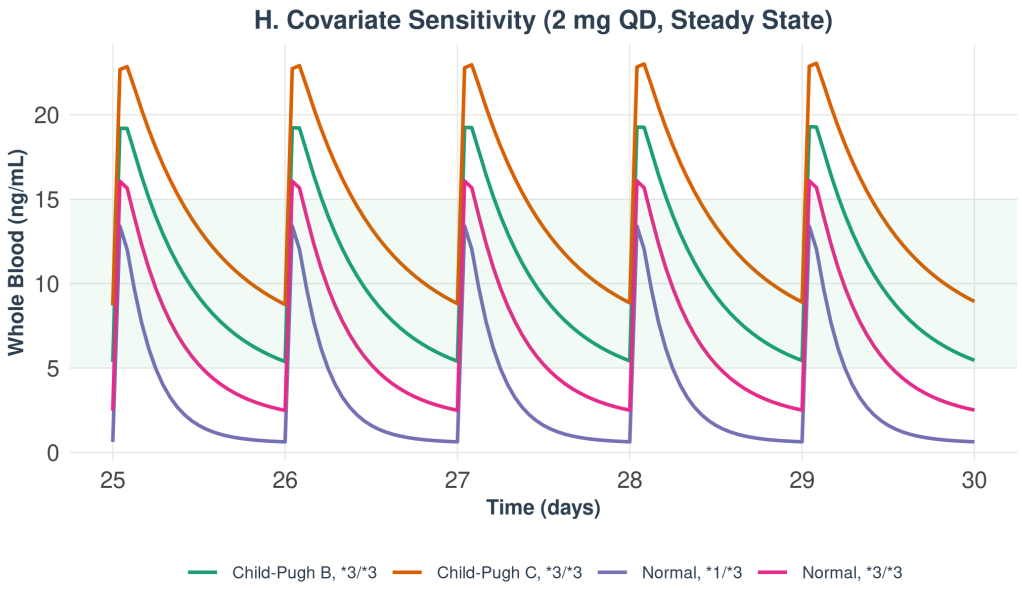

Figure 10: Covariate sensitivity at steady state (days 25–30, 2 mg QD, PopPK). CYP3A5 expressers show markedly lower exposure; hepatic impairment increases exposure dose-dependently.

Table 4: Covariate scenario metrics at steady state (PopPK, 2 mg QD).

Scenario	C_{avg} **(ng/mL)**	C_{trough} **(ng/mL)**	**Δ vs. baseline**
Normal hepatic, CYP3A5 *3/*3 (baseline)	6.51	2.51	—
Normal hepatic, CYP3A5 *1/*3 (expresser)	3.24	0.63	−50%
Child-Pugh B, CYP3A5 *3/*3	10.22	5.44	+57%
Child-Pugh C, CYP3A5 *3/*3	14.13	8.91	+117%

3.7 Weekly Dosing (Longevity Scenario)

Interest in rapamycin for longevity targets sub-immunosuppressive trough levels (<5 ng/mL). Figure 11 shows 6 mg weekly dosing. The tablet formulation produces $C_{max} = 41.5$ ng/mL with rapid decline to $C_{trough} = 0.55$ ng/mL at the end of the dosing interval ($C_{avg} = 2.86$ ng/mL). The large peak-trough ratio (∼75:1) is a direct consequence of the long dosing interval relative to the absorption phase: drug enters quickly but distributes and eliminates over the week.

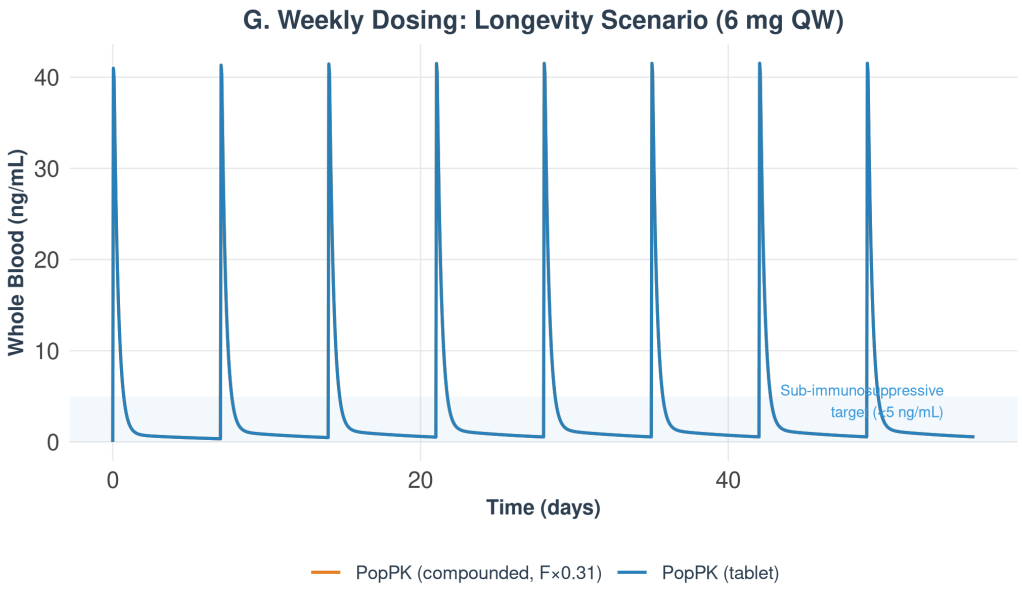

Figure 11: Weekly dosing for longevity (6 mg QW, PopPK). Blue band: sub-immunosuppressive target (<5 ng/mL). Average exposure is below immunosuppressive levels, but peak concentrations transiently exceed the transplant range.

4 Discussion

4.1 What the Two Models Agree On — and Where They Don't

Average exposure convergence is the expected result when both models are calibrated against the same clinical clearance and bioavailability data. The C_{avg} ratio of 1.00 (Table 1) confirms consistency.

The peak-trough divergence is more informative. The PopPK model's two-compartment structure uses empirical rate constants that were fit to whole-blood data; the peripheral compartment captures distribution kinetics without assigning them to specific tissues. The PBPK model distributes drug across explicit organs, and the high-K_p adipose compartment acts as a buffer that dampens central-compartment fluctuation. Neither model is "right" — the true peak-trough profile depends on sampling design and the specific patients studied. But the disagreement flags a clinically relevant question: is the PopPK trough of 2.5 ng/mL (which would be sub-therapeutic in transplant) more accurate than the PBPK trough of 5.9 ng/mL? Rich sampling studies at steady state would resolve this.

4.2 DDI Magnitude and Clinical Reality

The simulated DDI magnitudes track clinical observations well. Ketoconazole produces a simulated C_{avg} fold-change of $\sim$7.3$\times$ (47.2/6.5), slightly below the observed $\sim$10.9$\times$ AUC change. The discrepancy is expected: our model applies a single fold-change to clearance rather than mechanistically inhibiting CYP3A4 at the enzyme level, which underestimates the nonlinear interaction at the gut wall. The PBPK model's mechanistic DDI implementation (fold-change on CL_{int} and F_g) would better capture this, though we report only PopPK DDI results here for consistency across scenarios.

4.3 Population Variability and TDM

The finding that only 20% of patients achieve therapeutic troughs at 2 mg QD without individualization underscores why sirolimus requires TDM in transplant settings. The 5th–95th percentile spread (0.64–7.69 ng/mL) is driven by IIV in clearance (CV 38%) compounded by variability in weight and hematocrit. This is consistent with published PopPK analyses reporting similar IIV magnitudes [Golubović et al., 2019, Wu et al., 2012].

4.4 Limitations

1. B:P ratio treated as constant (35). True binding is saturable [ter Heine et al., 2018]; becomes relevant at supratherapeutic concentrations from DDIs.
2. P-glycoprotein efflux not explicitly modeled; F_g captures the net effect implicitly.
3. PopPK covariates are population-level. Individual Bayesian estimation from TDM levels would be preferred for clinical dosing.
4. Inter-occasion variability not modeled. Day-to-day PK variability is substantial in transplant patients.
5. No PK-PD link. A mechanistic connection from sirolimus concentrations to mTOR inhibition remains an identified literature gap [Shen et al., 2024].
6. Formulation bioavailability (F_1) in the PopPK model requires additional model code to properly scale absorbed dose; the current implementation has a known limitation for non-reference formulations.

5 Conclusion

We built two PK models of sirolimus from published data, ran them under matched conditions, and report their quantitative predictions side by side. They agree on average exposure (C_{avg} ratio 1.00) and diverge on peak-trough fluctuation — a structurally informative disagreement. The models reproduce expected DDI magnitudes, covariate effects, and population variability patterns. The interactive application allows real-time exploration of these scenarios. All literature synthesis was performed on the Edison Scientific platform.

Data and Code Availability

Shiny app source code, `mrgsolve` model files (C++), and simulation scripts are in the project repository. Edison project: `d19ffd55`.

References

Emoto, C., Fukuda, T., Cox, S., Christians, U., Vinks, A.A. Development of a PBPK model for sirolimus: predicting bioavailability based on intestinal CYP3A content. *CPT Pharmacometrics Syst. Pharmacol.*, 2:e59, 2013.

Zimmerman, J.J., Kahan, B.D. Pharmacokinetics of sirolimus in stable renal transplant patients after multiple oral dose administration. *J. Clin. Pharmacol.*, 37(5):405–415, 1997.

Zimmerman, J.J. Exposure-response relationships and drug interactions of sirolimus. *AAPS J.*, 6(4):e28, 2004.

Mahalati, K., Kahan, B.D. Clinical pharmacokinetics of sirolimus. *Clin. Pharmacokinet.*, 40(8):573–585, 2001.

ter Heine, R., et al. A pharmacological rationale for improved everolimus dosing in oncology and transplantation. *Br. J. Clin. Pharmacol.*, 84(7):1575–1586, 2018.

Golubović, B., et al. Exploring sirolimus pharmacokinetic variability using data available from routine clinical care of renal transplant patients — population pharmacokinetic approach. *J. Med. Biochem.*, 38(3):243–252, 2019.

Ferron, G.M., Mishina, E.V., Zimmerman, J.J., Jusko, W.J. Population pharmacokinetics of sirolimus in kidney transplant patients. *Clin. Pharmacol. Ther.*, 61(4):416–428, 1997.

Wu, K., et al. Nonlinear population pharmacokinetics of sirolimus in patients with advanced cancer. *CPT Pharmacometrics Syst. Pharmacol.*, 1:e17, 2012.

Lukas, J.C., Calvo, R., Zografidis, A., Ortega, I., Suárez, E. Simulation of sirolimus exposures and population variability immediately post renal transplantation: importance of the patient's CYP3A5 genotype in tailoring treatment. *Biopharm. Drug Dispos.*, 31(2–3):129–137, 2010.

Mao, J., et al. Dosing regimen recommendations for sirolimus in adult liver transplant recipients: insights from a population pharmacokinetic model. *Drug Des. Devel. Ther.*, 18:5975–5984, 2024.

Emoto, C., Fukuda, T., Venkatasubramanian, R., Vinks, A.A. The impact of CYP3A5*3 polymorphism on sirolimus pharmacokinetics: insights from predictions with a physiologically-based pharmacokinetic model. *Br. J. Clin. Pharmacol.*, 80(6):1438–1446, 2015.

Zimmerman, J.J., et al. PK of sirolimus in subjects with mild to moderate hepatic impairment. *J. Clin. Pharmacol.*, 45(12):1368–1378, 2005.

Zimmerman, J.J., et al. PK of sirolimus in subjects with severe hepatic impairment. *J. Clin. Pharmacol.*, 48(3):285–292, 2008.

Shen, G., Ren, S., Fan, H.-H., Moua, K.T.Y., Karolak, A., Rockne, R.C., Nakamura, R., Horne, D.A., Kanakry, C.G., Mager, D.E., McCune, J.S. Challenges with sirolimus experimental data to inform QSP model of post-transplantation cyclophosphamide regimens. *Clin. Transl. Sci.*, 17(8):e70014, 2024.